New Journal of Physics
The open access journal at the forefront of physics

Deutsche Physikalische Gesellschaft DPG IOP Institute of Physics

PAPER • OPEN ACCESS

Quantum probing beyond pure dephasing

To cite this article: Dario Tamascelli *et al* 2020 *New J. Phys.* **22** 083027

New Journal of Physics
The open access journal at the forefront of physics

Deutsche Physikalische Gesellschaft DPG
IOP Institute of Physics

Published in partnership with: Deutsche Physikalische Gesellschaft and the Institute of Physics

OPEN ACCESS

RECEIVED
2 March 2020

REVISED
26 May 2020

ACCEPTED FOR PUBLICATION
29 June 2020

PUBLISHED
11 August 2020

PAPER

Quantum probing beyond pure dephasing

Dario Tamascelli[1,2,6], Claudia Benedetti[1], Heinz-Peter Breuer[3,4] and Matteo G A Paris[1,5]

[1] Quantum Technology Lab, Dipartimento di Fisica 'Aldo Pontremoli', Università degli Studi di Milano, I-20133 Milano, Italy
[2] Institut für Theoretische Physik, Albert-Einstein-Allee 11, Universität Ulm, 89069 Ulm, Germany
[3] Physikalisches Institut, Albert-Ludwigs-Universität Freiburg, Hermann-Herder-Str. 3, 79104 Freiburg, Germany
[4] Freiburg Institute for Advanced Studies (FRIAS), Albert-Ludwigs-Universität Freiburg, Albertstr. 19, 79104 Freiburg, Germany
[5] INFN-Sezione di Milano, I-20133 Milano, Italy
[6] Author to whom any correspondence should be addressed.

E-mail: dario.tamascelli@unimi.it

Keywords: quantum metrology, open quantum systems, quantum probing, quantum Fisher information

Abstract

Quantum probing is the art of exploiting simple quantum systems interacting with a complex environment to extract precise information about some environmental parameters, e.g. the temperature of the environment or its spectral density. Here we analyze the performance of a single-qubit probe in characterizing Ohmic bosonic environments at thermal equilibrium. In particular, we analyze the effects of tuning the interaction Hamiltonian between the probe and the environment, going beyond the traditional paradigm of pure dephasing. In the weak-coupling and short-time regime, we address the dynamics of the probe analytically, whereas numerical simulations are employed in the strong coupling and long-time regime. We then evaluate the quantum Fisher information for the estimation of the cutoff frequency and the temperature of the environment. Our results provide clear evidence that pure dephasing is not optimal, unless we focus attention to short times. In particular, we found several working regimes where the presence of a transverse interaction improves the maximum attainable precision, i.e. it increases the quantum Fisher information. We also explore the role of the initial state of the probe and of the probe characteristic frequency in determining the estimation precision, thus providing quantitative guidelines to design optimized detection to characterize bosonic environments at the quantum level.

1. Introduction

Being able to characterize the properties of a complex environment through a simple, small and controllable quantum system is the leading scope of quantum probing [1–8]. This topic has a natural connection with the theory of quantum estimation, where the aim is to be able to precisely infer the value of unknown parameters through repeated measurements on the system of interest [9–14]. Indeed, the quality of a quantum probe can be evaluated through the error committed in characterizing parameters of the environment. The quantum Fisher information (QFI) is a measure of this error through the quantum Cramér–Rao bound. In order to extract the maximum information from a probing scheme, one needs to optimize the procedure over the preparation of the probe and over the kind of probe–environment interaction. We illustrate this problem by focusing on the estimation of the cutoff frequency and of the temperature of a bosonic bath with an Ohmic-like spectral density by using a single qubit as a quantum probe. This problem has already been addressed in reference [15] for the specific case of spin-boson model which induces a dephasing on the qubit dynamics [16], where it was shown that the optimal initial states of the probe are always the maximally coherent states (in the computational basis), e.g. the eigenstates of the σ_x Pauli matrix.

In this work we address the problem whether dephasing is the optimal interaction for the estimation of environmental parameters. As a matter of fact, in a pure dephasing dynamics only the coherences of the

system can be affected by the interaction with the environment. Other interactions, by allowing all the components of the reduced density matrix of the probe qubit to change, may lead to a larger gain of information on the environmental features, and thus to a more precise estimation of the inferred parameter(s). We show that this is indeed the case by considering the QFI related to the estimation of the cutoff frequency of the spectral density and the environmental temperature. In order to shed light on the role of the kind of system–environment interaction and of the probe's initial preparation on the ultimate estimation precision attainable, we analyze the behavior of the QFI as a function of time for different types of probe–bath interactions and different initial states of the probe. To determine the numerically exact evolution of the probe density matrix, we exploit the TEDOPA (time evolving density operator with orthogonal polynomiAls) algorithm [17–20], which allows for the efficient simulation of spin-boson models. While an exact analytic treatment is possible only for the specific case of pure dephasing dynamics, perturbative expansions, such as the time convolution-less (TCL) master equation [21, 22], are accurate only in the weak-coupling regime. Moreover, since in our setting we are interested in properties of the environment and not of the system, the general results derived in [23] are not applicable.

Our results show that while dephasing enhances the estimation precision at very short times, it is never optimal at longer times. The optimal initial state of the probe depends on the specific interaction chosen. We moreover bring evidence of the fact that the frequency of the probe qubit has a major impact on the ultimate estimation precision of environmental parameters. The paper is organized as follows. In section 1 we introduce the spin-boson model and the spectral density. In section 2 we define the quantum Fisher information. Section 4 is devoted to the derivation of the QFI in the weak-coupling limit. In section 4 we consider the arbitrary coupling case, and determine an approximate short-time evolution of the QFI in this scenario. The behavior of the QFI over longer times, obtained by numerical t-DMRG techniques, are discussed in section 4, before drawing our conclusion and offering perspectives.

2. The system

We consider a two-level system (TLS) interacting with a structured bosonic environment. For each environmental mode at frequency $\omega \geqslant 0$ the annihilation and creation operators $a_\omega, a_\omega^\dagger$ satisfy the commutation relations $[a_\omega, a_{\omega'}^\dagger] = \delta_{\omega,\omega'}$, $[a_\omega, a_{\omega'}] = [a_\omega^\dagger, a_{\omega'}^\dagger] = 0, \forall \omega, \omega' \geqslant 0$. The overall (system + environment) Hamiltonian is

$$H_{\mathrm{SE}}(\theta) = H_{\mathrm{S}} + H_{\mathrm{E}} + H_{\mathrm{I}}(\theta), \tag{1}$$

$$H_{\mathrm{S}} = \frac{1}{2}\omega_{\mathrm{S}}\sigma_z, \tag{2}$$

$$H_{\mathrm{E}} = \int_0^\infty \mathrm{d}\omega\, \omega\, a_\omega^\dagger a_\omega, \tag{3}$$

$$H_{\mathrm{I}}(\theta) = A_{\mathrm{S}}(\theta) \otimes G_{\mathrm{E}} \tag{4}$$

and the operators

$$A_{\mathrm{S}}(\theta) = \frac{\sigma_x}{2}\cos\ \theta + \frac{\sigma_z}{2}\sin\ \theta \tag{5}$$

$$G_{\mathrm{E}} = \int_0^\infty \mathrm{d}\omega\, \sqrt{J(\omega)}(a_\omega + a_\omega^\dagger) \tag{6}$$

model the system–environment interaction. Here and in what follows $\sigma_{x,y,z}$ are the Pauli matrices. When $\theta = \pi/2$, the dephasing model is recovered while for other values of θ the transverse (w.r.t. the system free Hamiltonian H_{S}) components come into play such that H_{S} and A_{S} no longer commute, leading to more involved dynamics for the probe qubit.

The function $J(\omega) : \mathbb{R}^+ \to \mathbb{R}^+$ is defined by the product of the interaction strength between the system and the environmental mode at frequency ω and the mode density around ω, and is usually referred to as the *spectral density* (SD). At time $t = 0$, system and environment are assumed to be in a factorized state $\rho_{\mathrm{SE}}(0) = \rho_{\mathrm{S}}(0) \otimes \rho_{\mathrm{E}}(0)$, where $\rho_{\mathrm{S}}(0)$ is an arbitrary state of the probe, $\rho_{\mathrm{E}}(0) = \otimes_\omega \exp\left(-\beta\omega a_\omega^\dagger a_\omega\right)/\mathcal{Z}_\omega$ is the thermal state of the environment at inverse temperature $\beta = 1/T$, and Z_ω is the partition function of the mode at frequency ω. Under these assumptions, the spectral density $J(\omega)$ entirely determines the open-system state $\rho_{\mathrm{S}}(t) = \mathrm{Tr}_{\mathrm{E}}\left[\rho_{\mathrm{SE}}(t)\right]$, since it determines the two-time correlation function (TTCF)

$$\begin{aligned} C(t) &= \langle G_{\mathrm{E}}(t) G_{\mathrm{E}}(0)\rangle_{\rho_{\mathrm{E}}(0)} = \langle \mathrm{e}^{\mathrm{i}H_{\mathrm{E}}t} G_{\mathrm{E}} \mathrm{e}^{-\mathrm{i}H_{\mathrm{E}}t} G_{\mathrm{E}}\rangle_{\rho_{\mathrm{E}}(0)} \\ &= \int_0^{+\infty} \mathrm{d}\omega J(\omega) \left[n_\beta(\omega) \mathrm{e}^{\mathrm{i}\omega t} + (1 + n_\beta(\omega)) \mathrm{e}^{-\mathrm{i}\omega t}\right] \\ &= \int_{-\infty}^{+\infty} \mathrm{d}\omega \mathrm{e}^{\mathrm{i}\omega t} j_\beta(\omega). \end{aligned} \tag{7}$$

where $n_\beta(\omega) = 1/(\mathrm{e}^{\beta\omega} - 1)$ and

$$j_\beta(\omega) = \frac{1}{2}\left[1 + \coth\left(\frac{\beta\omega}{2}\right)\right] [J(\omega)\Theta(\omega) - J(-\omega)\Theta(-\omega)] \tag{8}$$

is a non-negative function that we will refer to as to the *thermalized spectral density* [17]. Since the environment is initially in a (Gaussian) thermal state, multi-time correlations are all functions of the TTCF $C(t)$ alone.

In this work we will consider Ohmic spectral densities of the form

$$J(\omega) = \frac{\lambda}{\omega_c^{s-1}} \omega^s \mathrm{e}^{-\frac{\omega}{\omega_c}}, \tag{9}$$

where λ is an overall constant, $s > 0$ is the Ohmicity parameter, ω_c indicates the bath cutoff frequency, and we assumed an exponential form of the cutoff. The corresponding TTCF reads

$$C_{\lambda,s,\omega_c,\beta}(t) = \frac{\lambda s! \omega_c^2}{(1 + \mathrm{i}\omega_c t)^{s+1}} + \lambda\omega_c^2 \left(-\frac{1}{\beta\omega_c}\right)^{s+1} \left[\Phi^{(s)}\left(1 + \frac{1 + \mathrm{i}\omega_c t}{\beta\omega_c}\right) + \Phi^{(s)}\left(1 + \frac{1 - \mathrm{i}\omega_c t}{\beta\omega_c}\right)\right], \tag{10}$$

$\Phi^{(s)}(z)$ being the polygamma function of order s.

In the following we will assume $\omega_c = 1$ and express time and frequency in dimensionless ω_c-based units. We also use natural units $\hbar = k_{\mathrm{B}} = c = 1$ throughout the paper.

3. Quantum Fisher information

Consider a family of quantum states $\{\rho_\eta\}$ depending on the parameter η which we want to estimate. The ultimate precision of any unbiased estimator $\widehat{\eta}$ of the parameter η is given by the single-shot quantum Cramèr–Rao inequality:

$$\sigma^2[\widehat{\eta}] \geqslant \frac{1}{Q(\eta)}, \tag{11}$$

where σ^2 is the variance of the estimator and $Q(\eta)$ is the quantum Fisher information defined as:

$$Q(\eta) = \mathrm{Tr}[\rho_\eta L_\eta^2]. \tag{12}$$

L_η is the symmetric logarithmic derivative implicitly defined by $\frac{\partial\rho_\eta}{\partial\eta} = \frac{1}{2}\{L_\eta, \rho_\eta\}$ and $\{\cdot\}$ denotes the anticommutator. The QFI thus quantifies the ability to estimate an unknown parameter by posing a lower bound to the variance of the estimator $\widehat{\eta}$. The problem to accurately infer the value of an unknown parameter is strictly connected to the ability to discriminate between states ρ_η and $\rho_{\eta+\delta\eta}$, where $\delta\eta$ is an infinitesimal small deviation. The larger the QFI, he higher is the ability to distinguish between neighboring states (in η), and the smaller is the error associated to the estimation procedure. Not surprisingly, thus, $Q(\eta)$ can be expressed in terms of the Uhlmann fidelity [24, 25], which unveils the distinguishability between quantum states that are infinitesimally distant [26]. The fidelity is defined as

$$\mathcal{F}(\rho_1, \rho_2) = \left(\mathrm{Tr}\sqrt{\sqrt{\rho_1}\,\rho_2\,\sqrt{\rho_1}}\right)^2 \tag{13}$$

and its connection to the QFI is expressed by the relation [27, 28]

$$Q(\eta, t) = \lim_{\delta\eta\to 0} \frac{8\left(1 - \sqrt{\mathcal{F}\left(\rho_\eta(t), \rho_{\eta+\delta\eta}(t)\right)}\right)}{\delta\eta^2}. \tag{14}$$

In what follows we will also exploit an alternative, but equivalent, definition of the QFI, which may be introduced as follows: given the time-local generator $\mathcal{L}(t)$ of the master equation

$$\frac{\mathrm{d}\rho(t)}{\mathrm{d}t} = \mathcal{L}(t)[\rho(t)], \tag{15}$$

the corresponding linear dynamical map is given by

$$\Lambda(t) = T_{\leftarrow} \mathrm{e}^{\int_0^t \mathrm{d}\tau \mathcal{L}(\tau)} = \sum_{k=0}^{\infty} \int_0^t \mathrm{d}t_1 \mathcal{L}(t_1) \int_0^{t_1} \mathrm{d}t_2 \mathcal{L}(t_2) \ldots \int_0^{t_k} \mathrm{d}t_k \mathcal{L}(t_k). \tag{16}$$

Given the orthonormal basis of operators $\{\tau_k\}_{k=0}^3 = \{\mathbb{1}/\sqrt{2}, \sigma_x/\sqrt{2}, \sigma_y/\sqrt{2}, \sigma_z/\sqrt{2}\}$, and the Hilbert–Schmidt scalar product $\langle \xi, \chi \rangle \equiv \mathrm{Tr}\left(\xi^\dagger \chi\right)$, any linear map $\mathcal{M}$ acting on a qubit state ρ can be represented through a 4×4 matrix

$$\mathcal{M}[\rho] = \sum_{\alpha\beta=0}^{3} D^{\mathcal{M}}_{\alpha\beta} \langle \tau_\beta, \rho \rangle \tau_\alpha \qquad D^{\mathcal{M}}_{\alpha\beta} = \langle \tau_\alpha, \mathcal{M}[\tau_\beta] \rangle. \tag{17}$$

Analogously, a state ρ can be written as a 4×1 column vector $\widetilde{\boldsymbol{r}} = (\langle \mathbb{1}, \rho \rangle = 1, \langle \sigma_x, \rho \rangle, \langle \sigma_y, \rho \rangle, \langle \sigma_z, \rho \rangle)^T$ containing the coefficients $\langle \tau_\alpha, \rho \rangle$ of the decomposition

$$\rho = \frac{1}{\sqrt{2}} \boldsymbol{\tau} \cdot \widetilde{\boldsymbol{r}} = \sum_{\alpha=0}^{3} \langle \tau_\alpha, \rho \rangle \tau_\alpha = \frac{1}{2} \left(\mathbb{1} + \sum_{\alpha=x,y,z} \langle \sigma_\alpha, \rho \rangle \right), \tag{18}$$

where the terms $\langle \sigma_\alpha, \rho \rangle, \alpha = x, y, z$ are the components of the Bloch vector associated to ρ. Given a completely positive trace preserving (CPTP) dynamical map $\Lambda(t)$, the most general form of the matrix D^Λ associated with it is

$$D^\Lambda = \begin{pmatrix} 1 & \mathbf{0}^T \\ \boldsymbol{\nu} & V \end{pmatrix}, \tag{19}$$

where $\mathbf{0}^T$ is a three-dimensional row vector, $\boldsymbol{\nu}$ is a real 3 dimensional column vector and V is a 3×3 real matrix. By construction, therefore, the column $\boldsymbol{\nu}$ induces a state independent translation of the Bloch vector $\boldsymbol{r} = (\langle \sigma_x, \rho \rangle, \langle \sigma_y, \rho \rangle, \langle \sigma_z, \rho \rangle)^T$, whereas V describes rotations, reflections and contraction of $\boldsymbol{r}$, so that

$$D^\Lambda \widetilde{\boldsymbol{r}} = (1, \boldsymbol{\nu} + V\boldsymbol{r})^T. \tag{20}$$

As shown in [29], given an initial state $\widetilde{\boldsymbol{r}}(0)$, the quantum Fisher information associated to an unknown parameter η of the η-dependent dynamical map $\Lambda_\eta(t) = \Lambda(t)$ can be expressed as:

$$Q(\eta, t) = |\dot{D}^{\Lambda(t)} \widetilde{\boldsymbol{r}}(0)|^2 + \frac{(D^{\Lambda(t)} \widetilde{\boldsymbol{r}}(0) \cdot \dot{D}^{\Lambda(t)} \widetilde{\boldsymbol{r}}(0))^2}{2 - |D^{\Lambda(t)} \widetilde{\boldsymbol{r}}(0)|^2}, \tag{21}$$

where $\dot{D}^{\Lambda(t)}$ indicates the derivative with respect to the parameter η.

4. Weak-coupling limit

The determination of the QFI requires the knowledge of the reduced system state $\rho_S(t) = \mathrm{Tr}_E[\rho_{SE}(t)]$, or equivalently of the dynamical map $\mathcal{M}(t)$ such that $\rho_S(t) = \mathcal{M}(t)\rho_S(0)$. Such reduced state and dynamical map, as we mentioned before, are exactly analytically available in the spin-boson setting (equations (1)–(9)) only for the specific case $\theta = \pi/2$, corresponding to a pure dephasing dynamics ($[H_S, H_I(\pi/2)] = 0$) [16]. For arbitrary values of θ, instead, an analytically exact description of the evolved state $\rho_S(t)$ of the open system is, in general, not available. In this section we study the short-time evolution of the probe qubit, and the corresponding behavior of the accuracy limits, as determined by the QFI, of the estimation of unknown environmental parameters. A closed form of the master equation governing the dynamics of the probe qubit system interacting with a bosonic environment as described by (1), can be perturbatively derived in the weak coupling limit. By following the procedure described in [23], involving a second-order time convolutionless (TCL) expansion, we end up with the master equation

$$\frac{\mathrm{d}\rho(t)}{\mathrm{d}t} = \mathcal{L}(t)[\rho(t)] = -i\left[H_S + H^{LS}(t), \rho(t)\right] + \sum_{j,k=\pm,z} b_{kj}(t) \left(\sigma_k \rho(t) \sigma_j - \frac{1}{2} \left\{ \sigma_j^\dagger \sigma_k, \rho(t) \right\} \right), \tag{22}$$

where $\sigma_\pm = (\sigma_x \pm \mathrm{i}\sigma_y)/2$. Introducing the function

$$\Gamma(\xi, t) = \int_0^t \mathrm{d}\tau \mathrm{e}^{\mathrm{i}\xi\tau} C(\tau), \tag{23}$$

the time-dependent coefficients of the Lamb-shift Hamiltonian correction $H^{\mathrm{LS}}(t)$ and of the dissipative part $b_{kj}(t)$ read (see equation (36) of [23])

$$\begin{aligned}
b_{zz}(t) &= \frac{\sin^2(\theta)}{2}\Re[\Gamma(0,t)]\\
b_{++}(t) &= \frac{\cos^2(\theta)}{2}\Re[\Gamma(-\omega_{\mathrm{S}},t)]\\
b_{--}(t) &= \frac{\cos^2(\theta)}{2}\Re[\Gamma(\omega_{\mathrm{S}},t)]\\
b_{+-}(t) = b^*_{-+}(t) &= \frac{\cos^2(\theta)}{4}(\Gamma(-\omega_{\mathrm{S}},t) + \Gamma^*(\omega_{\mathrm{S}},t))\\
b_{z+}(t) = b^*_{+z}(t) &= \frac{\sin(\theta)\cos(\theta)}{4}(\Gamma(0,t) + \Gamma^*(-\omega_{\mathrm{S}},t))\\
b_{z-}(t) = b^*_{-z}(t) &= \frac{\sin(\theta)\cos(\theta)}{4}(\Gamma(0,t) + \Gamma^*(\omega_{\mathrm{S}},t))\\
H_{11}(t) &= \frac{\cos^2(\theta)}{4}\Im[\Gamma(\omega_{\mathrm{S}},t)]\\
H_{10}(t) = H^*_{01}(t) &= \frac{-i\,\sin(\theta)\cos(\theta)}{4}\left(\Re[\Gamma(0,t)] - \frac{1}{2}\left(\Gamma^*(-\omega_{\mathrm{S}},t) + \Gamma(\omega_{\mathrm{S}}(t))\right)\right)\\
H_{11}(t) &= \frac{\cos^2(\theta)}{4}\Im[\Gamma(-\omega_{\mathrm{S}},t)],
\end{aligned} \tag{24}$$

where $\Re[\cdot], \Im[\cdot]$ indicate the real resp. imaginary part, c^* the complex conjugate of c and $H^{\mathrm{LS}}_{ij}(t) = \langle i|H^{\mathrm{LS}}(t)|j\rangle, \quad i,j = 0,1$. Our aim here is to obtain the short-time solution of the master equation (22). To this end, it is sufficient to consider only the terms of $D^{\Lambda(t)}$ up to some order k in t.

In order to get an insight into the dependence of the QFI, in the very initial phase of the dynamics, on the initial condition $\rho_{\mathrm{S}}(0)$ and on the interaction angle θ, we start by considering the (2nd order) Dyson expansion of $D^{\Lambda(t)}$ with only terms up to t^2. The resulting super-operator matrix $D^{\Lambda(t)}_{(2)}$ reads

$$D^{\Lambda(t)}_{(2)} = \begin{pmatrix}
1 & 0 & 0 & 0\\
0 & 1 - \frac{t^2}{2}(\zeta(0)\sin^2(\theta) + \omega_{\mathrm{S}}^2) & -t\omega_{\mathrm{S}} & \frac{1}{4}\zeta(0)t^2\,\sin(2\theta)\\
0 & t\omega_{\mathrm{S}} & 1 - \frac{t^2}{2}\left(\zeta(0) + \omega_{\mathrm{S}}^2\right) & 0\\
0 & \frac{t^2}{4}\zeta(0)\sin(2\theta) & 0 & 1 - \frac{t^2}{2}\zeta(0)\cos^2(\theta)
\end{pmatrix}, \tag{25}$$

where $\zeta(n)$ indicates the nth moment of the spectral density, i.e.

$$\zeta(n) = \frac{1}{i^n}\frac{\mathrm{d}^n}{\mathrm{d}t^n}C(t)\bigg|_{t\to 0}. \tag{26}$$

Since the QFI is convex, we restrict our attention to pure initial states; moreover, for the sake of simplicity, we restrict the initial states to lie in the $x-z$ plane, so that the initial condition can be parametrized by a single angle α as

$$\boldsymbol{r}_0(\alpha) = (\cos(\alpha), 0, \sin(\alpha))^T. \tag{27}$$

By exploiting (21), it is easy to determine the QFI for the estimation of an arbitrary environment parameter η. The leading order term is proportional to t^2 and reads

$$Q_{(2)}(\eta, t) = \frac{t^2}{4}\sin^2(\alpha - \theta)\frac{(\partial_\eta\zeta(0))^2}{\zeta(0)}, \tag{28}$$

where we indicate by $Q_{(k)}$ the QFI corresponding to $D^{\Lambda(t)}_{(k)}$, i.e. the matrix obtained by keeping the terms up to t^k of the Dyson expansion (16). For arbitrarily chosen, but fixed, environmental parameters the steepest increase of $Q(\eta, t)$, at short times, is thus provided by the choices $\alpha - \theta = \pi/2 + k\pi,\ k \in \mathbb{Z}$. If a pure

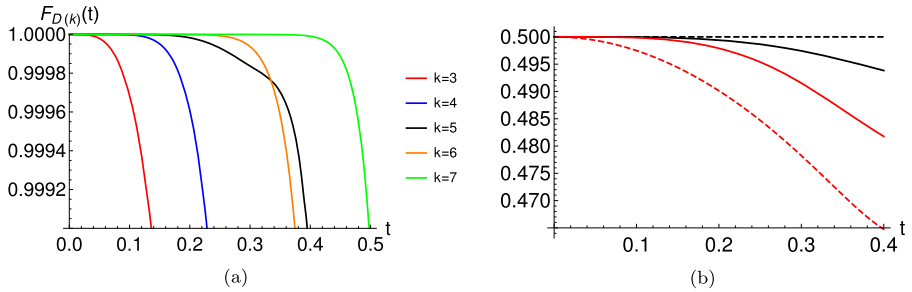

Figure 1. In both frames: $\lambda = 1, s = 1, T = 0.1, \omega_S = 5$ (remind that $\omega_c = 1$), initial state $\rho_S(0) = |+\rangle\langle+|$. Panel (a): the fidelity (13) between the numerical solution $\rho_S^{TCL}(t) = \Lambda(t)\rho_S(0)$ of the TCL master equation (22) and $\rho_S^{D(k)}(t) = D_{(k)}^{\Lambda(t)}\rho_S(0)$ as a function of time for different values of the time-expansion order k. Panel (b): the evolution of the excited state population (black) and of the absolute value of the coherence (red) when the initial state $\rho_S(0)$ is evolved under a pure dephasing dynamics ($\theta = \pi/2$, dashed) and a completely transverse dynamics ($\theta = 0$, solid).

dephasing dynamics ($\theta = \pi/2$) is considered, for example, the initial states maximising the initial increase in the QFI (28) correspond to $\alpha = k\pi, \quad k \in \mathbb{Z}$, namely the eigenstates of σ_x, which are already known to be the optimal ones in this case. In the presence of a purely transverse system–environment interaction ($\theta = 0$), instead, the initial state maximising the initial growth of the QFI is given by the choice $\alpha = \pi/2 + k\pi, \quad k \in \mathbb{Z}$, i.e. the eigenstates of σ_z. We moreover point out that different combinations of α and θ resulting in the same value $\alpha - \theta$ will lead to the same initial increase of the QFI.

We notice that (28) is independent on the system frequency ω_S; such dependence emerges only if higher order Dyson expansions $D_{(k)}^{\Lambda(t)}$ and the corresponding $Q_{(k)}(\eta, t)$ are considered. This means that ω_S dependent terms can contribute to the QFI, and thus be used as another control parameter of the probe qubit, only for sufficiently large times, or stronger system–environment couplings. This can be seen by analyzing the matrix form for the generator $\mathcal{L}(t)$, derived by using

$$D_{(3)}^{\mathcal{L}(t)} = \begin{pmatrix} 0 & \mathbf{0} \\ \boldsymbol{\mu}_{(3)}(t) & W_{(3)}(t) \end{pmatrix}, \tag{29}$$

with $\mathbf{0}$ the three-dimensional zero vector,

$$\boldsymbol{\mu}_{(3)}(t) = \frac{t^3\,\zeta(1)\omega_S}{6}\left(\sin(2\theta), 0, -2\,\cos^2(\theta)\right)^T, \tag{30}$$

and the matrix $W_{(3)}(t)$ is fully defined in appendix A. $D_{(3)}^{\mathcal{L}(t)}$ reveals that such dependence on ω_S appears indeed only for $k \geqslant 3$ (or $k \geqslant 4$ if $D_{(k)}^{\Lambda(t)}$ is considered).

Moreover, it is interesting to notice from equation (19) that the dynamical map $\Lambda(t)$ loses its unital character, namely $\Lambda(t)[\mathbb{1}] \neq \mathbb{1}$, but for $\theta = \pi/2 + k\pi, k = 1, 2, \ldots$, i.e. for pure dephasing dynamics. Since the translation term $\boldsymbol{\mu}(t)$ in the generator $D_{(3)}^{\mathcal{L}(t)}$ is proportional to t^3, however, the lowest order contribution to the translational part $\boldsymbol{\nu}(t)$ (see (20)) to the dynamics is of order t^4. For very short times, therefore, the translations of the Bloch vector will be negligible, and the map will be approximately unital. On the other side, this fact suggests that the dynamics of the Bloch vector over longer times, or in the presence of a stronger coupling to the environment, will be affected by environment-dependent translations; this can affect the dependence of the probe state on the environmental parameters, and lead to an increase of the QFI related to the estimation of these latter. We moreover observe that, by avoiding the high temperature limit $\beta \to 0$ used in [23] our setting allows to address the estimation of system or environmental parameters in any temperature range.

Beside providing an analytic insight on some of the features of the dynamical map, the Dyson expansions $D_{(k)}^{\Lambda(t)}$ turn out to be most useful for the numerical analysis of the dependence of the QFI on the interaction and initial state parameters in the weak-coupling/short-time regime we are discussing here. For the computation of the QFI $Q(\eta, t)$ by means of (14) the evolved states $\rho_\eta(t)$ and $\rho_{\eta+\delta\eta}(t)$ are needed. Such states can be determined by numerical integration of the TCL master equation (22). However, for the small increments $\delta\eta$ required for good finite-difference approximations of the infinitesimal increment limit $\delta\eta \to 0$, numerical instabilities can arise. In fact, $\rho_\eta(t)$ and $\rho_{\eta+\delta\eta}(t)$ start from the same initial state, and at very short times/weak coupling, the difference between the evolved states is typically very small. It is easy to check that such instabilities are much more pronounced, and appear over longer time-intervals, in the presence of energy-exchange type of interaction ($\theta = 0$ in our setting) alone: energy-exchange processes typically occur on longer times (see figure 1(b)).

In what follows we will therefore adopt a different approach and determine the evolution of the probe qubit by means of $D_{(7)}^{\Lambda(t)}$. On the one hand, it provides excellent approximation of the dynamical map determined by the TCL master equation up to $t \approx 0.4$, as exemplified in figure 1(a); on the other, it allows for an analytic derivation of the QFI by means of (21).

In order to quantify the optimality of pure dephasing we introduce the ratio

$$R_t(\eta, \theta, \alpha) = \frac{Q^{\theta,\alpha,\omega_S}(\eta, t) - Q^{\frac{\pi}{2},0,\omega_S}(\eta, t)}{Q^{\frac{\pi}{2},0,\omega_S}(\eta, t)}, \tag{31}$$

namely the relative difference between the QFI determined by the evolution of the probe system having free dynamics determined by $H_S = \frac{1}{2}\omega_S\sigma_z$ initially in the state $\boldsymbol{r}_0(\alpha)$ and interaction Hamiltonian $H_I(\theta)$ and the QFI at the same time provided by a pure dephasing dynamics of the probe qubit starting from the (dephasing-optimal) initial state $\rho_S(0) = |+\rangle\langle+|$, as a figure of merit for the estimation of the environmental parameter η. We have $R > 0$ when a strategy outperform the performance of dephasing.

We apply our setting to the study of the QFI associated with the short-time estimation of the bosonic bath (inverse) temperature T (β) and of the cutoff frequency ω_c, i.e. $Q(\beta, t)$ and $Q(\omega_c, t)$, respectively. An identical procedure can be clearly applied to other environmental parameters, such as λ and s.

Our calculations show that a pure dephasing dynamics acting on the initial state $\boldsymbol{r}_0(0)$ is optimal for temperature estimation: other combinations of the interaction angle θ and of the initial state angle α lead to smaller $Q(\beta, t)$[7]. This can be seen in figures B1(a)–(c), which shows the ratio $R_t(\beta, \theta, \alpha)$ at time $t = 0.35$. The behavior is qualitatively the same at any $t \leqslant 0.35$ and for different values of the Ohmicity parameter s and whenever $\omega_c \gtrsim \omega_S$. As clearly visible in frames (a)–(c) of figure B1 (see solid and dashed lines), initial states 'orthogonal' to the interaction angle ($\alpha = \theta \pm \pi/2$) lead in general to higher values of the QFI. This is particularly evident in the case $\omega_S \ll \omega_c$ (figure B1(a)) where any choice $\alpha = \theta + \pi/2$ leads to the same $Q(\beta, t)$, as already predicted by the short-time expansion (28). As the system frequency ω_s is increased, instead, only the dephasing with initial state angle $\alpha = 0$ is optimal. The QFI is instead minimized when the initial state is parallel to the interaction angle ($\alpha = \theta$).

The situation is different when $Q(\omega_c, t)$ is considered (frames (d)–(f) of figure B1). For $\omega_S \geqslant \omega_c$ a purely transverse interaction term and an initial condition parallel to the z axis outperforms pure dephasing at the considered time $t = 0.35$ (see figure B1(f)) and, as we will see in the next section, for longer times. For shorter times, instead, pure dephasing dynamics with the initial state corresponding to $\alpha = 0$ remains optimal (not shown). This suggests that energy exchanges between the system and the environment, which typically occur on longer times, see figure 1(b), can provide additional information on the bath cutoff energy ω_c. As in the case of temperature estimation, initial conditions orthogonal to the interaction direction lead to larger values of the QFI, whereas initial conditions parallel to the interaction direction correspond to smaller values of the QFI.

5. Long times/arbitrary coupling

The analysis of the previous section was limited to the weak-coupling regime and short times. Intuition suggests, on the other hand, that a stronger or longer interaction of the probe qubit with the environment could allow for a larger information gain on the environmental features, and therefore to an increase of the ultimate precision of the estimation of environmental parameters. Moreover, by extending the interaction time, the exchange of energy between system and environment which typically occur on time-scales much longer than the one characteristic of pure dephasing, can become more relevant. An indication in this direction was already provided by the behavior of $R(\omega_c, \theta, \alpha)$ for $\omega_S \gg \omega_c$ (see figure B1(f)).

As well known, an analytic solution of the spin-boson model (1) for arbitrary times and coupling strength is however available only for pure dephasing. For general directions of the system–environment interaction term a numerical solution is needed.

In this section, we explore, by numerical means, the behavior of the QFI associated to the temperature ($\eta = T$) and cutoff frequency ($\eta = \omega_c$) estimation for different directions of the interaction term $H_I(\theta)$ and initial states $r_0(\alpha)$. More specifically, we use the T-TEDOPA [17] method in order to determine $\rho_S(t)$ in a numerically exact way. We refer the reader to appendix B for a streamlined description of T-TEDOPA and

[7] The optimality of pure dephasing dynamics together with the choice $\alpha = 0$ is not clearly visible in frame (a) of figure 2: the points ($\theta = \pi/2$, $\alpha = 0$) and ($\theta = \pi/2$, $\alpha = \pi$) are indeed the only ones where $Q(\beta, t) = 1$; the other points along the black lines always correspond, in this frame, to slightly smaller values of $Q(\beta, t)$.

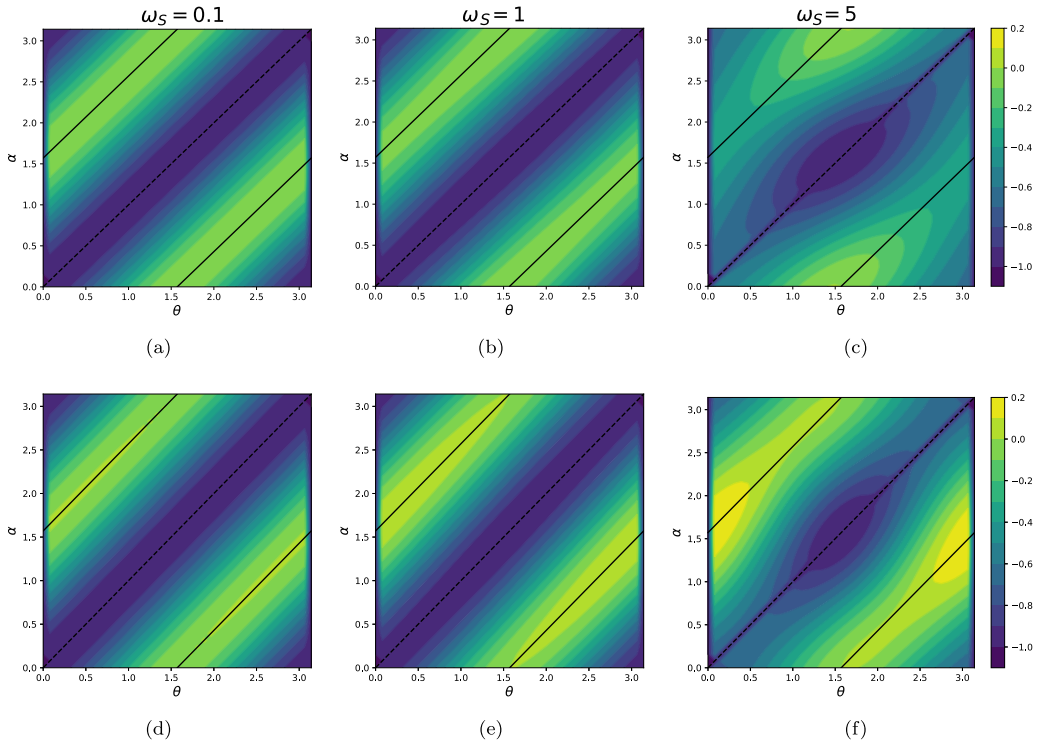

Figure 2. All frames: $\lambda = 1, s = 1, T = 0.07 (\beta = 1/T \approx 14.3), t = 0.35$. Panels (a)–(c): temperature estimation with $R_t(\beta, \theta, \alpha)$ for $\omega_S = 0.1$, 1 and 5 (remind that $\omega_c = 1$). Panels (d)–(f): cutoff frequency estimation with $R_t(\omega_c, \theta, \alpha)$ for the same three values of ω_S. Black solid lines, corresponding to the points $(\theta, \alpha = \theta \pm \pi/2)$, and black dashed lines, corresponding to the points $(\theta, \alpha = \theta)$, are used as a guide to the eye to locate the parameters regions corresponding respectively to the larger and smaller values of the ratio $R_t(\eta, \theta, \alpha)$.

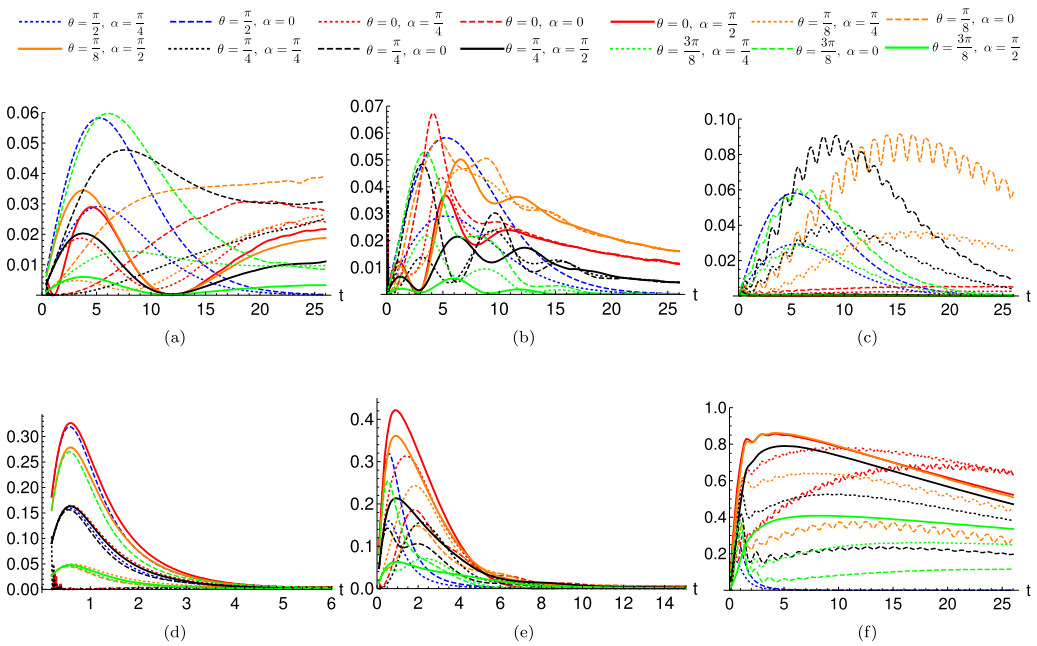

Figure 3. All plots: $q(\eta, t) = Q(\eta, t)/t$ as a function of t, $\lambda = 1, s = 1, T = 0.07$ (remind that $\omega_c = 1$). Frames (a)–(c) temperature estimation ($\eta = \beta$) for (a) $\omega_S = 0.1$, (b) $\omega_S = 1$, (c) $\omega_S = 5$. Frames (d)–(f): cutoff frequency estimation ($\eta = \omega_C$) for (d) $\omega_S = 0.1$, (e) $\omega_S = 1$, (f) $\omega_S = 5$.

all the details needed to reproduce our results and to extend the analysis to other environmental parameters not discussed here, such as the overall coupling λ and the Ohmicity s.

In our numerical analysis we limited ourselves to consider the three initial states corresponding to $\alpha = 0$, $\alpha = \pi/4$ and $\alpha = \pi/2$ and interaction angles $\theta \in [0, \pi/2]$. The considered initial states and interaction angles are enough to see a rich variety of behaviors of the QFI, and in particular to show that a

pure dephasig interaction is never optimal for the estimation of bath parameters if we consider dynamics over long times, allowing for system–environment energy exchange processes to occur.

Clearly enough, the numerical approach does not allow for an analytic derivation of the QFI, as equivalently defined in equations (14) or (21), which would require a truly infinitesimal $\delta\eta$. We instead adopted a finite-difference approach: we derived, for any considered initial condition and interaction angle, the matrices $\rho_\eta(t)$ and $\rho_{\eta+\delta\eta}(t)$ by changing the estimated parameter in the spectral density by $\delta\eta$. In what follows we set $\delta\eta = 10^{-4}$, which provides converged values of the QFI (smaller values of $\delta\eta$ lead to the same result). It is worth noting here that we are interested in the behavior of the QFI over times much longer than those considered in the previous section, so that such finite-different approach can be safely adopted: while the numerical instabilities due to the closeness, at short times, of the states $\rho_\eta(t)$ and $\rho_{\eta+\delta\eta}(t)$ are still there, they do not affect the computation of the QFI at longer times, where, in general, the distance between the two evolved states is larger.

Instead of looking directly at the quantum Fisher information, we analyze the behavior of the QFI rescaled with time, i.e.

$$q(\eta, t) = \frac{Q(\eta, t)}{t}. \tag{32}$$

In a metrological context, where time is a resource, it is important to be able to perform the measurements in a short time or, otherwise stated, it is important to have a large repetition rate for the measurement. The quantity $q(\eta, t)$ takes into account the fact that a large QFI at long times may be less advantageous with respect to a lower QFI at shorter times. High values for the quantity $q(\eta, t)$ thus indicates a large information gain in a metrological sense. Figures 3(a)–(c) show the behavior of $q(\beta, t)$ in time, for different combination of the (θ, α) angles and for different values of the system frequency ω_S. The time-evolution of the rate q for pure dephasing dynamics for the optimal initial state corresponding to the choice $\alpha = 0$ is clearly independent of the system frequency ω_S; it exhibits a maximum at $t \approx 5$ and steadily decreases, getting close to zero around $t = 25$. For other values of θ the behavior of $q(\beta, t)$ shows a strong dependence on ω_S and there are combinations of interaction angle θ, initial state angle α and times leading to higher values of $q(\beta, t)$ than the one achievable with pure dephasing dynamics. This is particularly evident if, for example, $\omega_S = 5$ is considered. It follows that, even in cases where time is considered as a metrological resource, pure-dephasing is not the optimal choice. The choice $\theta = \pi/8$ and $\alpha = 0$, for example, leads to a globally better rate q. This contrasts with the results obtained for short times (figures 2(a)–(c)), where pure-dephasing dynamics resulted to be always optimal.

The sub-optimality of pure dephasing dynamics is even more evident when the estimation of the cutoff parameter ω_c is addressed. Figures 2(e)–(f) already showed that, in this case, there are interaction angles and initial states outperforming pure dephasing. Figures 3(d)–(e) show that, when longer times are considered, the choice $\theta = 0, \alpha = 0$ leads to a 33% larger value of $q(\omega_c, t)$ for $t \approx 1$ and $\omega_S = 1$ w.r.t. pure dephasing, whereas the same choice of the interaction and initial state angles leads to a 100% larger value of $q(\omega_c, t)$ when $\omega_S = 5$. Qualitatively similar behaviors are obtained for super- ($s > 1$) and sub- ($s < 1$) Ohmic spectral densities (not shown).

6. Conclusions

In this paper we have investigated whether engineering the interaction Hamiltonian may improve the precision of quantum probing. In particular, we have considered a qubit probe interacting with a bosonic Ohmic environment and have addressed the effects of going beyond pure dephasing on the precision of estimation of environmental parameters such as the temperature, or the cutoff frequency of the environment spectral density. We have analyzed the behavior of the maximal extractable information, as quantified by the quantum Fisher information, for different initial preparations of the probe and system–bath interaction.

Our results provide clear evidence that pure dephasing interaction is not optimal in general, except for very short times. The presence of a transverse interaction may indeed improve the maximum attainable precision in several working regimes. From a physical point of view, our results show that the exchange of energy between the system and the environment plays a major role in determining the QFI and this is especially evident in the strong-coupling regime, see e.g. figure 3.

Besides the dynamics, we have also analyzed the role of the kinematics of the probe in determining the precision of the estimation. In particular, we have analyzed the role of the initial state of the probe and that of its characteristic frequency. Our results illustrate the complex interplay among the different features of the probe and provide quantitative guidelines to design optimal detection schemes characterizing bosonic environments at the quantum level.

Acknowledgments

We thank Andrea Smirne for useful discussions. MGAP is member of INdAM-GNFM. HPB acknowledges support from the Joint Project 'Quantum Information Processing in Non-Markovian Quantum Complex Systems' funded by the Freiburg Institute for Advanced Studies (FRIAS, University of Freiburg) and the Institute of Advanced Research (IAR, Nagoya University). CB, DT, and MGAP acknowledge support from UniMi through the APC initiative. DT acknowledges support from UniMi through the 'Sviluppo UniMi' project.

Appendix A. Generator and dynamical map

The matrix form of the generator $\mathcal{L}(t)$, defined in (22) with coefficients given by (24) can be derived by using (17) and keeping only terms up to t^3.

$$D^{\mathcal{L}(t)}_{(3)} = \begin{pmatrix} 0 & \mathbf{0} \\ \boldsymbol{\mu}_{(3)}(t) & W_{(3)}(t) \end{pmatrix}, \tag{A1}$$

with $\mathbf{0}$ the three-dimensional zero vector,

$$\boldsymbol{\mu}_{(3)}(t) = \frac{t^3\,\zeta(1)\omega_S}{6}\left(\sin(2\theta), 0, -2\,\cos^2(\theta)\right)^T, \tag{A2}$$

and

$$W_{(3)}(t) = \begin{pmatrix} \frac{1}{6}\zeta(2)t^3\,\sin^2(\theta) - \zeta(0)t\,\sin^2(\theta) & -\omega_S & \frac{1}{2}\zeta(0)t\,\sin(2\theta) - \frac{1}{12}t^3\left(\zeta(0)\omega_S^2 + \zeta(1)\omega_S + \zeta(2)\right)\sin(2\theta) \\ \frac{1}{2}t^2\omega_S(\zeta(0)\cos^2(\theta)) + \omega_S & \frac{1}{6}t^3\left(\zeta(0)\omega_S^2\cos^2(\theta) + \zeta(2)\right) - \zeta(0)t & \frac{1}{8}t^2(2\zeta(0)\omega_S + \zeta(1))\sin(2\theta) \\ \frac{1}{12}t^3(\zeta(1)\omega_S - \zeta(2))\sin(2\theta) + \frac{1}{2}\zeta(0)t\,\sin(2\theta) & -\frac{1}{8}\zeta(1)t^2\,\sin(2\theta) & \frac{1}{6}t^3\left(\zeta(0)\omega_S^2 + \zeta(2)\right)\cos^2(\theta) - \zeta(0)t\,\cos^2(\theta) \end{pmatrix} \tag{A3}$$

It is worth noticing that the generator of the translations $\boldsymbol{\mu}_{(3)}(t)$ depends on the first moment $\zeta(1)$ of the spectral density. It is possible to show, by direct inspection of higher-order generators $D^{\mathcal{L}(t)}_{(k)}$, $k > 3$ that the generators of the translations depend only on the odd-moments $\zeta(2n+1)$. For spectral densities belonging to the Ohmic family, such odd moments are independent of the temperature.

Appendix B. TEDOPA algorithm

To simulate the evolution of the spin-boson model, we resorted to the recently proposed thermalized time evolving density matrix with orthogonal polynomials (T-TEDOPA) algorithm. In this section we briefly present the T-TEDOPA scheme and refer to [17] for a more detailed presentation of the algorithm. Clearly enough, other numerical methods such as hierarchical equation of motion (HEOM) [30, 31], or the recently proposed transformation to auxiliary oscillators (TSO) [32, 33], can be applied, as long as high enough accuracy is guaranteed.

T-TEDOPA is a certifiable and numerically exact method [18–20] to efficiently treat finite-temperature open quantum system dynamics. T-TEDOPA first extends the bosonic environment by including negative frequency modes. The initial state of the extended environment, governed by the Hamiltonian $H_E^{\text{ext}} = \int_{-\infty}^{+\infty} \mathrm{d}\omega\; a_\omega^\dagger a_\omega$, is set to the (pure) vacuum state $|0\rangle_E$ (i.e. $a_\omega|0\rangle_E = 0 \quad \forall\omega \in \mathbb{R}$). The spectral density $J(\omega)$ is then replaced by a the *thermalized* spectral density

$$J_\beta(\omega) = \frac{J^{\text{ext}}(\omega)}{2}\left[1 + \coth\left(\frac{\beta\omega}{2}\right)\right] \tag{B1}$$

with $J^{\text{ext}}(\omega) = \text{sign}(\omega)J(|\omega|)$. Since $J_\beta(\omega)$ is a measure, i.e. a positive valued function, on $\mathbb{R}$, it is possible to determine a family of polynomials $p_{\beta,n}(\omega)$ orthogonal w.r.t. the measure $\mathrm{d}\mu_\beta = J_\beta(\omega)\mathrm{d}\omega$, and define new creation and annihilation operators $c^{(\dagger)}_{n,\beta}$ through a unitary transformation:

$$U_{\beta,n}(\omega) = \sqrt{J_\beta(\omega)}p_{\beta,n}(\omega), \tag{B2}$$

$$c^{(\dagger)}_{\beta,n} = \int_{-\infty}^{+\infty} \mathrm{d}\omega\; U_{\beta,n}(\omega)a^{(\dagger)}_\omega. \tag{B3}$$

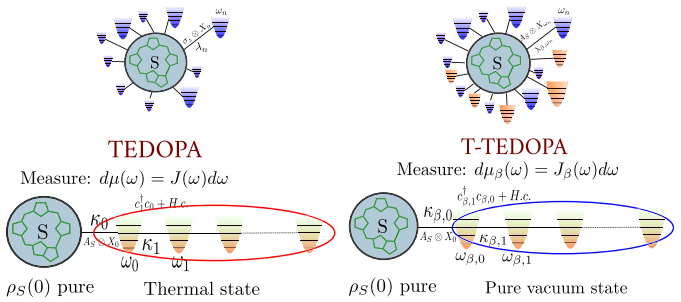

Figure B1. A pictorial scheme of the TEDOPA and T-TEDOPA transformations.

As for standard TEDOPA, thanks to the three-term recurrence relation satisfied by the polynomials $p_{\beta,n}(\omega)$, the $H_{\mathrm{SE}}(\theta)$ Hamiltonian (1) is mapped into a chain Hamiltonian $H^{\mathrm{C}}(\theta) = H_{\mathrm{S}} + H_{\mathrm{E}}^{\mathrm{C}} + H_{\mathrm{I}}^{\mathrm{C}}(\theta)$ where

$$H_{\mathrm{I}}^{\mathrm{C}}(\theta) = \kappa_{\beta,0} A(\theta)(c_0 + c_0^\dagger) \tag{B4}$$

$$H_{\mathrm{E}}^{\mathrm{C}} = \sum_{n=0}^{+\infty} \omega_{\beta,n} c_n^\dagger c_n + \sum_{n=1}^{+\infty} \kappa_{\beta,n}(c_{n-1} c_n^\dagger + c_{n-1}^\dagger c_n), \tag{B5}$$

with $A(\theta)$ defined as in (5). The transformation therefore maps the environment into a semi-infinite one-dimensional chain of oscillators with nearest-neighbor interactions and the coefficients $\omega_{\beta,n}$, $\kappa_{\beta,n}$ are, respectively, the temperature dependent chain oscillators frequencies and coupling strengths, directly related to the coefficients of the recurrence relation defined by the orthogonal polynomials $p_{\beta,n}(\omega)$. These latter are typically computed by means of stable numerical routines [34]. This transformation from the spin-boson model to a one-dimensional geometry is depicted in figure B1.

In a second step this emerging configuration is treated by time evolving block decimation (TEBD) method. TEBD generates a high fidelity approximation of the time evolution of a one-dimensional system subject to a nearest-neighbor Hamiltonian with polynomially scaling computational resources. TEBD does so by dynamically restricting the exponentially large Hilbert space to its most relevant subspace thus rendering the computation feasible [35].

TEBD is essentially a combination of an MPS description [36] for a one-dimensional quantum system and an algorithm that applies two-site gates that are necessary to implement a Suzuki–Trotter time evolution [37]. Together with MPS operations such as the application of measurements this yields a powerful simulation framework. An extension to mixed states is possible by introducing a matrix product operator (MPO) to describe the density matrix, in complete analogy to an MPS describing a state [36, 38]. Such an extension is indeed not needed in our simulations. As a matter of fact we consider only pure initial states of the system. The environmental initial state is, instead, a thermal state. However, by applying T-TEDOPA, we are able to shift the thermal contributions from the initial state of the chain to temperature-dependent chain coefficients, and initialize the chain in the (pure) vacuum state. This provides us with the possibility of using a pure state (MPS) description of the overall system–environment state, with major computational advantage. We refer to [17] for a more detailed comparison between T-TEDOPA and TEODPA.

A last step is necessary to adjust this configuration further to suit numerical needs. The number of levels for the environment oscillators can be restricted to a value $d_{\max}$ to reduce required computational resources. A suitable value for $d_{\max}$ is related to the sites average occupation which, in turn, depends on the environment structure and temperature. In our simulations we set $d_{\max} = 12$: this value provides converged results for all the examples provided. The Hilbert space dynamical reduction performed by TEBD is determined to the *bond dimension*. The optimal choice of this parameter depends on the amount of long range correlations in the system. For all the simulations used in this work, a bond dimension $\chi = 50$ provided converged results. At last, we observe that the mapping described above produces a semi-infinite chain that must be truncated in order to enable simulations. In order to avoid unphysical back-action on the system due to finite-size effects, i.e. reflections from the end of the chain, the chain has to be sufficiently long to completely give the appearance of a 'large' reservoir. These truncations can be rigorously certified by analytical bounds [39]. For the examples provided in the paper, chains of $n = 150$ sites are more than enough to see no boundary effect.

As to further optimize our simulations, we augmented our TEDOPA code with a reduced-rank randomized singular value decomposition (RRSVD) routine [40, 41]. Singular value decomposition is at the

heart of the dimensionality reduction TEBD relies on. RRSVD is a randomized version of the SVD that provides an improved-scaling SVD, with the same accuracy as the standard state of the art deterministic SVD routines.

ORCID iDs

Dario Tamascelli https://orcid.org/0000-0001-6575-4469
Claudia Benedetti https://orcid.org/0000-0002-8112-4907
Heinz-Peter Breuer https://orcid.org/0000-0002-4030-6720
Matteo G A Paris https://orcid.org/0000-0001-7523-7289

References

[1] Elliott T J and Johnson T H 2016 *Phys. Rev.* A **93** 043612
[2] Norris L M, Paz-Silva G A and Viola L 2016 *Phys. Rev. Lett.* **116** 150503
[3] Benedetti C and Paris M G 2014 *Phys. Lett.* A **378** 2495
[4] Benedetti C, Buscemi F, Bordone P and Paris M G A 2014 *Phys. Rev.* A **89** 032114
[5] Tamascelli D, Benedetti C, Olivares S and Paris M G A 2016 *Phys. Rev.* A **94** 042129
[6] Cosco F, Borrelli M, Plastina F and Maniscalco S 2017 *Phys. Rev.* A **95** 053620
[7] Sone A and Cappellaro P 2017 *Phys. Rev.* A **96** 062334
[8] Usui A, Buča B and Mur-Petit J 2018 *New J. Phys.* **20** 103006
[9] Paris M G A 2009 *Int. J. Quantum Inf.* **07** 125
[10] Pinel O, Jian P, Treps N, Fabre C and Braun D 2013 *Phys. Rev.* A **88** 040102
[11] Genoni M G, Paris M G A, Adesso G, Nha H, Knight P L and Kim M S 2013 *Phys. Rev.* A **87** 012107
[12] Tóth G and Apellaniz I 2014 *J. Phys. A: Math. Theor.* **47** 424006
[13] Troiani F and Paris M G A 2018 *Phys. Rev. Lett.* **120** 260503
[14] Seveso L, Benedetti C and Paris M G A 2019 *J. Phys. A: Math. Theor.* **52** 105304
[15] Benedetti C, Salari Sehdaran S, Zandi M H and Paris M G A 2018 *Phys. Rev.* A **97** 012126
[16] Breuer H-P and Petruccione F 2002 *The Theroy of Open Quantum Systems* (Oxford: Oxford University Press)
[17] Tamascelli D, Smirne A, Lim J, Huelga S F and Plenio M B 2019 *Phys. Rev. Lett.* **123** 090402
[18] Prior J, Chin A W, Huelga S F and Plenio M B 2010 *Phys. Rev. Lett.* **105** 050404
[19] Woods M P, Groux R, Chin A W, Huelga S F and Plenio M B 2014 *J. Math. Phys.* **55** 032101
[20] Woods M P, Cramer M and Plenio M B 2015 *Phys. Rev. Lett.* **115** 130401
[21] Shibata F, Takahashi Y and Hashitsume N 1977 *J. Stat. Phys.* **17** 171
[22] Breuer H P, Kappler B and Petruccione F 2001 *Ann. Phys.* **291** 36
[23] Haase J F, Smirne A, Kołodyński J, Demkowicz-Dobrzański R and Huelga S F 2018 *New J. Phys.* **20** 053009
[24] Uhlmann A 1976 *Rep. Math. Phys.* **9** 273
[25] Jozsa R 1994 *J. Mod. Opt.* **41** 2315
[26] Bures D J C 1969 *Trans. Am. Math. Soc.* **135** 199
[27] Braunstein S L and Caves C M 1994 *Phys. Rev. Lett.* **72** 3439
[28] Safránek D 2017 *Phys. Rev.* A **95** 052320
[29] Zhong W, Sun Z, Ma J, Wang X and Nori F 2013 *Phys. Rev.* A **87** 022337
[30] Taniumura Y and Kubo R 1989 *J. Phys. Soc. Jpn.* **58** 101
[31] Taniumura Y 2006 *J. Phys. Soc. Jpn.* **75** 082001
[32] Mascherpa F, Smirne A, Somoza A D, Fernández-Acebal P, Donadi S, Tamascelli D, Huelga S F and Plenio M B 2020 *Phys. Rev.* A **101** 052108
[33] Tamascelli D, Smirne A, Huelga S F and Plenio M B 2018 *Phys. Rev. Lett.* **120** 030402
[34] Gautschi W 1994 *ACM Trans. Math. Softw.* **20** 21
[35] Vidal G 2004 *Phys. Rev. Lett.* **93** 040502
[36] Schollwöck U 2011 *Ann. Phys.* **326** 96
[37] Suzuki M 1990 *Phys. Rev. Lett.* **146** 319
[38] Zwolak M and Vidal G 2004 *Phys. Rev. Lett.* **93** 207205
[39] Woods M, Cramer M and Plenio M 2015 *Phys. Rev. Lett.* **115** 130401
[40] Tamascelli D, Rosenbach R and Plenio M B 2015 *Phys. Rev.* E **91** 063306
[41] Kohn L, Tschirsich F, Keck M, Plenio M B, Tamascelli D and Montangero S 2018 *Phys. Rev.* E **97** 013301